ELSEVIER

Catalysis Today 23 (1995) 201–218

CATALYSIS TODAY

What can we observe in zeolite related materials by HRTEM?

Osamu Terasaki [a,*], Tetsu Ohsuna [b]

[a] *Department of Physics, Tohoku University, Sendai 980-77, Japan*

[b] *Department of Materials Science, Iwaki Meisei University, Iwaki 970, Japan*

Abstract

High-resolution electron microscopy, both scanning and transmission, has given a big contribution to the study of fine structures of zeolites on an atomic scale. Recent progress by the authors on the fine structures of zeolites is reviewed.

1. Introduction

Zeolites are crystalline alumino-silicate materials with the nominal composition $M_{x/m}[Al_xSi_{1-x}O_2]nH_2O$, where M is a cation of valence m. Their frameworks are built from corner-shared TO_4-tetrahedra (T stands for Si or Al) to produce channels or cavities (hereafter called spaces) of molecular dimensions inside the crystals [1]. Zeolites are mostly synthesized as a fine powder of ca. 1 μm in size. If they are free from defects, their structures can be determined by the X-ray powder diffraction method. However, they often contain different types of defects and, moreover, their chemical and physical properties deviate from those expected from their ideal structures because of defects. Zeolites form many different families in which common structure building units for the frameworks are found, and therefore they have a strong tendency to form intergrowths between different structures within the same families, such as ERI/OFF in ABC-6 [2,3] and EMT/FAU in FAU families [4,5]. There are also many polymorphs where structures are well described by the stacking sequence of the sheets such as BEA [6] and titanosilicate ETS-10 [7,8]. It is becoming more and more important to understand their surface structures not only for synthesizing high quality or novel zeolites in order to provide better catalysts but also in order to better understand the catalytic reaction on the surfaces. As for catalysts or catalyst supports, zeolites are modified by the incorporation of metal clusters. In this case, it is vitally important to determine the size of the clusters and locate their positions, whether they are in the spaces of zeolites or on the external surface, and to check whether the crystallinity of the zeolites is well held after the treatment of incorporation of metal clusters.

Electron microscopy (scanning electron microscopy (SEM), electron diffraction (ED) and in particular high-resolution transmission electron microscopy (HRTEM)) provides the crucial starting point for characterizing the fine structures and solving such complex structures. SEM is good for characterizing macroscopic features especially crystal morphology and surface steps. The details of the fine structure and the nature of disorder are directly revealed by HRTEM images [6–8]. But there are two big dis-

* Corresponding author.

SSDI 0920-5861(94)00164-2

advantages for EM study of zeolites, firstly zeolites are quite electron-beam sensitive [9] and secondly HRTEM images suffer from artificial electron optical effects [10–12].

In this review, we will show some of our studies on the fine structures of zeolites and try to show how EM is powerfully applied.

2. Experimental

Zeolites were as-synthesized or crushed in an agate mortar, dispersed in acetone (otherwise specified) and placed on a microgrid for HRTEM and ED observations. Pt metal particles were evaporated on the crystals on a grid by sputtering for Pt/LTL. The particle size and density are controlled by the change of distance between the grid and the Pt-metal plate and by the sputtering time. For SEM observations, the powders as-synthesized were dispersed in acetone using ultrasound and drops placed on a conductive tape. SEM images were taken on an S-5000 microscope with a field emission gun (FEG) operated at a low accelerating voltage between 2 to 5 kV without metal coating. Most of the HRTEM and ED patterns were taken on 400 kV EM with a spherical aberration $C_s = 1.0$ mm. 200 kV EM with $C_s = 0.7$ mm and 1 MV EM with $C_s = 11.0$ mm were also used.

3. Fine structure of zeolites

3.1. HRSEM

Recent progress in SEM equipped with FEG coefficient is enormous especially in obtaining high-resolution images from non-conductive materials such as zeolites. Using a low accelerating voltage has two advantages. The first is in providing selective information from the surface region because of the small penetration depth for low energy electrons, and the second is that the ratio of incident electrons to secondary ones decreases toward 1 and therefore 'charging effects' are not serious from zeolites as the accelerating voltage decreases. However, in order to obtain high-resolution images at low accelerating voltages, high brightness of the electron source with high coherence is essential. Here we confine ourselves to the case of HRSEM images of FAU, and three examples are shown in Fig. 1a, b and c.

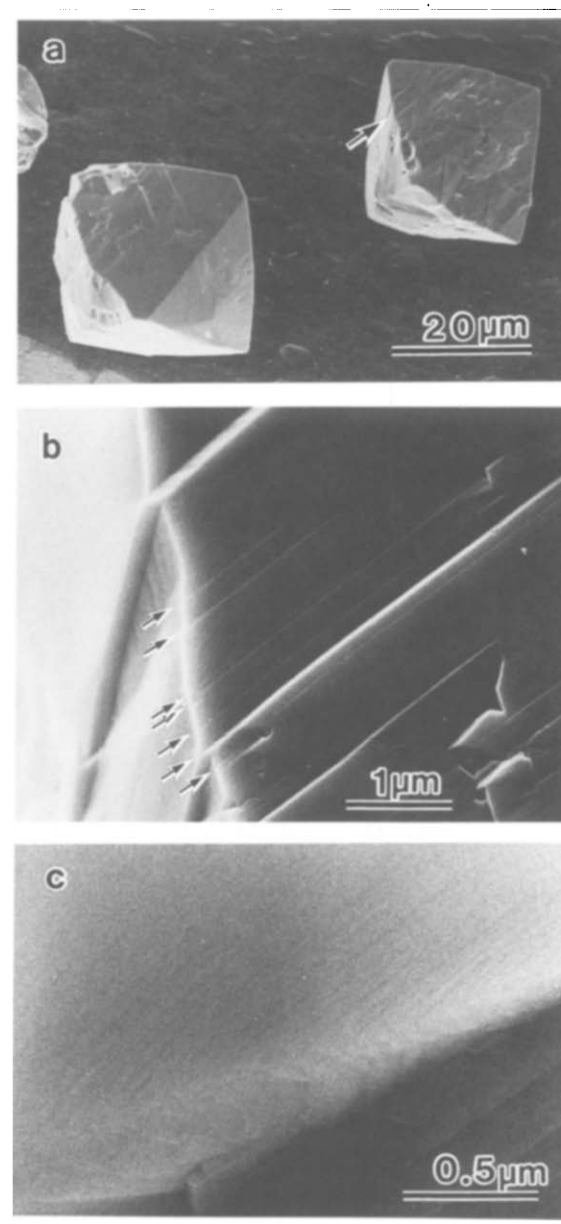

Fig. 1. SEM images of FAU. Low magnification image of single crystal FAU (a) and an enlarged image of a part indicated by an arrow in a (b). HRSEM image showing surface steps (c).

These are low magnifications of single crystals of FAU (Fig. 1a), and a high magnification of a part of the right crystal of Fig. 1a in order to observe twin structure, especially its density (Fig. 1b). A few of the twins are indicated in the image by arrows. Fig. 1c shows surface steps observed on one of the $\{111\}_c$ surface of a single crystal, although the contrast is not good but it is quite discernible. From this image it is difficult to tell the height of the steps, unless a high-resolution SEM image is taken with an incidence parallel to the surface after tilting the crystal by ca. 90°.

3.2. HRTEM

3.2.1. LTL system

3.2.1.1. LTL as-synthesized. LTL contains a one-dimensional channel with 12-membered rings and the channels are well separated by the framework atoms. It has a space group P6/mmm and the unit cell dimensions are $a = 18.4$ Å, $c = 7.5$ Å. The crystal shape of the LTL used in this experiment is a cylindrical plate with diameters ranging from 0.1 to 3 μm and aspect ratios (diameter/height) ranging from ca. 2 to 5. Fig. 2a shows a schematic drawing of a projection of the framework structure along the [001] and Fig. 2b shows a corresponding HRTEM image of LTL. All channels in Fig. 2a, that is, six 8-membered rings and six 6-membered rings as well as the main ones, are distinctly observed in the image. Even one planar defect may destroy the one-dimensional character. Indeed, it is quite common in LTL to find the growth of one crystal onto or into another in a wedge shape and such defects are produced during the process of crystal growth [13,14]. Although the orientation relation between the crystallites is easily determined by electron diffraction (ED) patterns, HRTEM observation is essential to determine the spatial relationship between them. We have reported coincidence boundaries of $\sqrt{13}\times\sqrt{13}$ $R32.2°$ where one crystal (B) grows on another (A) with rotation of ca. 32° (a non-multiple of 60°) along the c axis, i.e., the channel direction [13]. This is shown in Fig. 3a. More than 90% of the one-dimensional channels are blocked in this case. The HRTEM image of Fig. 3b also shows a few different boundaries or faults. Two different 'Moiré' patterns are observed in the image at the regions of A and B. The left part (A) corresponds to overlapped crystals with ca. 10° rotation and the right part (B) to ca. 4° rotation [14].

During an investigation of the surface structure of (001) or the surface step by taking an HRTEM image along [100] which is perpendicular to the channel direction, we observed a damage process by electrons. The sequence of HRTEM images taken with this direction are shown in Fig. 4a, b and c under an electron irradiation. The crystal thickness of the top layer along the electron beam incidence, [100], may be too large to be thought of as surface structure. From these images it is very clear that degradation of LTL under an electron beam is not uniform. The crystallinity at the top and bottom surfaces of (001) stays longer than the middle part, and the crystal shape changes from a cylindrical plate to a cotton-reel shape (to form waist) as schematically shown in Fig. 4d as previously reported by Treacy and Newsam [15]. They also confirmed the previous observation that the rate of vitrification depends sensitively on the degree of hydration [9,13].

3.2.1.2. Pt/K-LTL. Pt containing LTL has attracted a lot of attention as catalysts. The accurate characterization of the Pt particles, which consists of the determination of the particle sizes and their location relative to zeolite framework structures, is the main issue in order to understand their chemical properties. HRTEM is a powerful and direct method for this purpose, but it is not easy to determine decisively whether the particles are inside the channels of the zeolite or outside the crystals. This is because the strong contribution from the framework in the HRTEM image masks the contrast from the clusters especially when electrons are incident parallel to the direction of the channels in order to obtain a structure image and the electron-optical effect causes artifact, and furthermore zeolites are quite electron-beam sensitive as mentioned previously. In order to over-

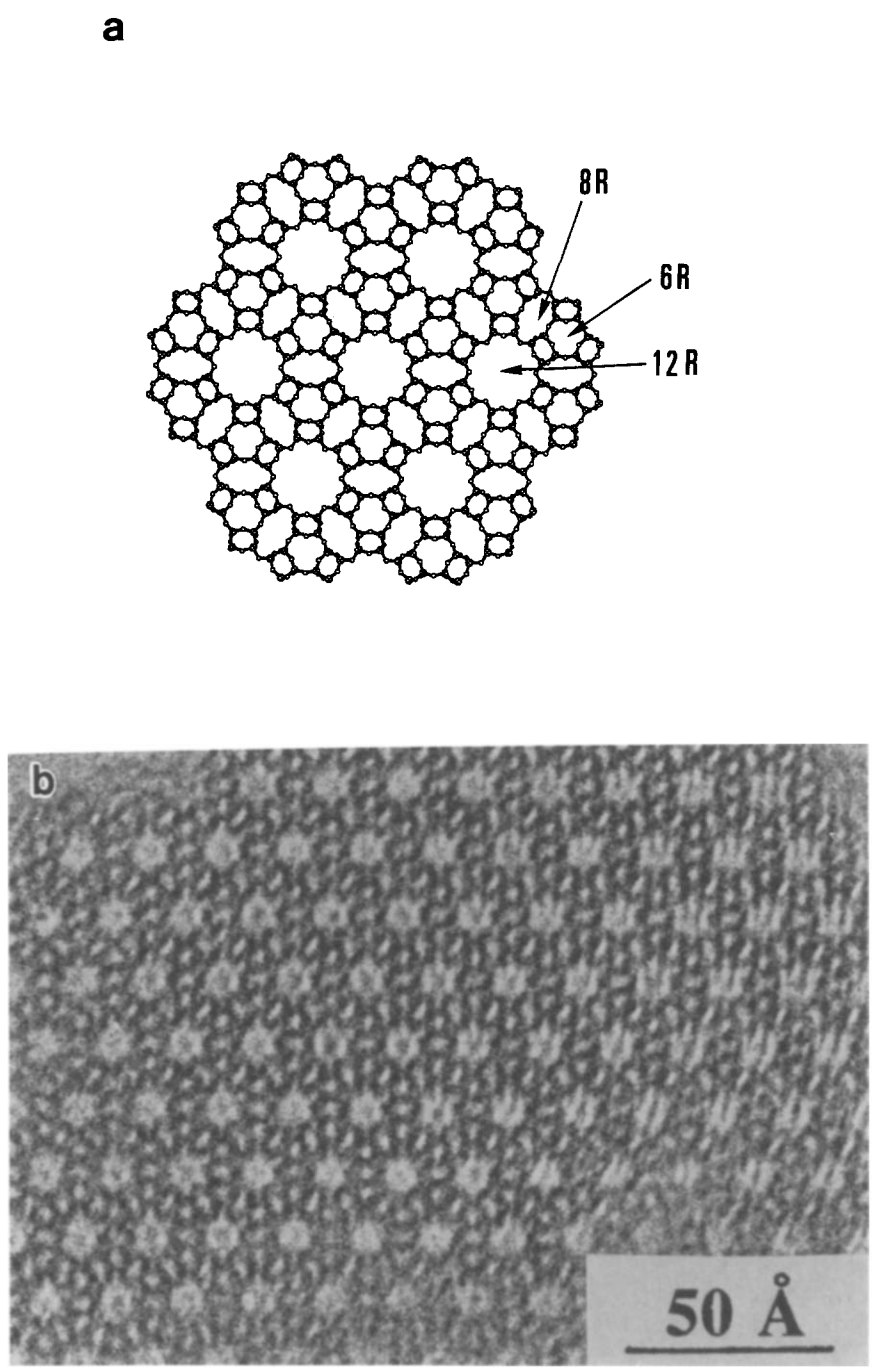

Fig. 2. A schematic drawing of the framework structure of LTL viewed along [001] (a) and a corresponding HRTEM image of LTL taken on 400 kV EM (b).

come this difficulty, a few ways have been proposed: image processing [10–12], HRTEM observation of serial ultra thin-sectioned specimens [16] and the Z-contrast method [17,18]. It is normally believed that the particles are inside, if the particles are not observed on the surface in the HRTEM image when looking at the direction perpendicular to the channel. A question then

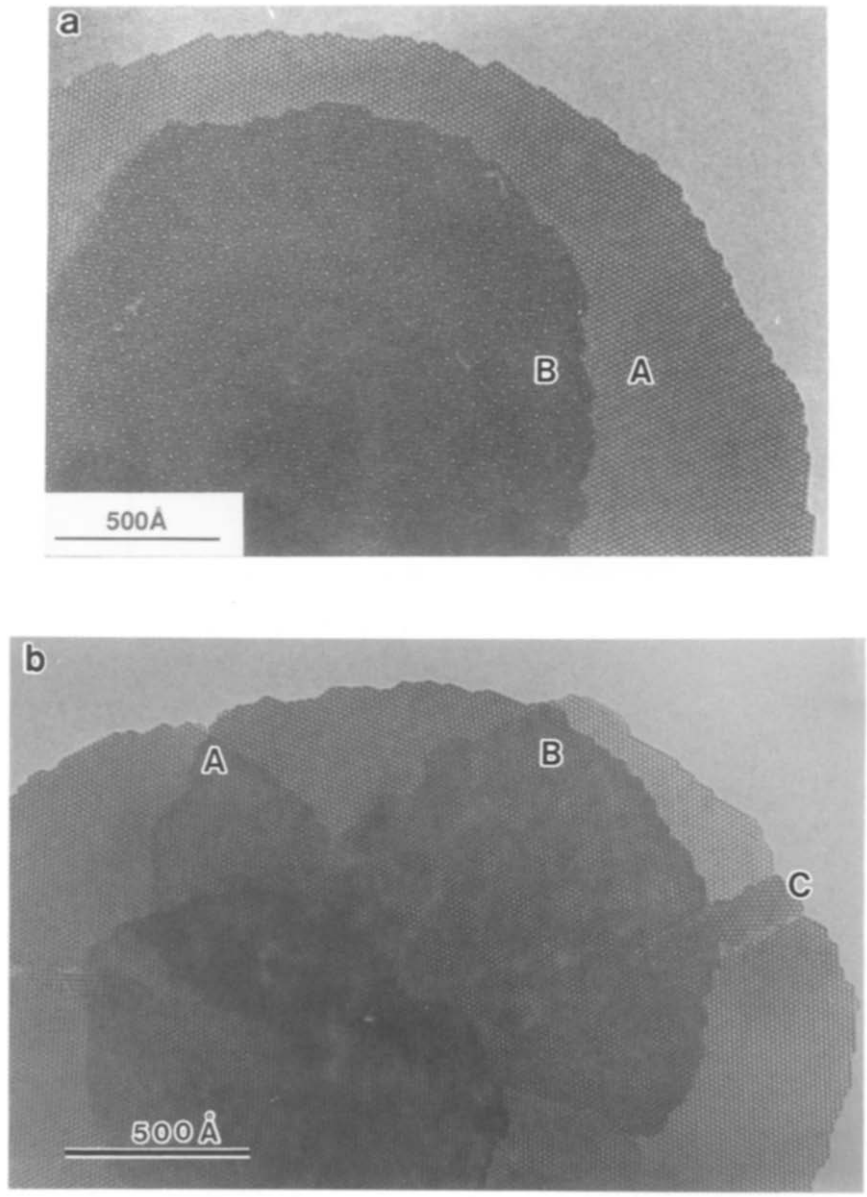

Fig. 3. HRTEM images of LTL taken on 400 kV EM with [001]. Coincidence boundary (a) and other boundaries (b) where Moiré effects are due to overlapping crystals with a rotation angle of ca. 10° (A), 4° (B) and a tilt boundary of ca. 30° (C) is also observed.

arises, how can small particles be observed in HRTEM images under certain conditions? The following is a part of our answer to this question.

As mentioned in the experimental section, the Pt particles are sputtered on the outer surface of the crystals, therefore we are sure the particles are on the external surfaces in this experiment. With the electron beam parallel to the channels, we can observe a contrast from the Pt clusters which are on the (001) plane, if the particles are larger than approximately 30 Å and this is more than four times larger than the channel aperture. A series of HRTEM image of Pt/LTL taken with [001] under electron beams are shown in Fig. 5a, b and c. If the crystal is in contact to a microgrid through the (001) plane, the morphology change induced

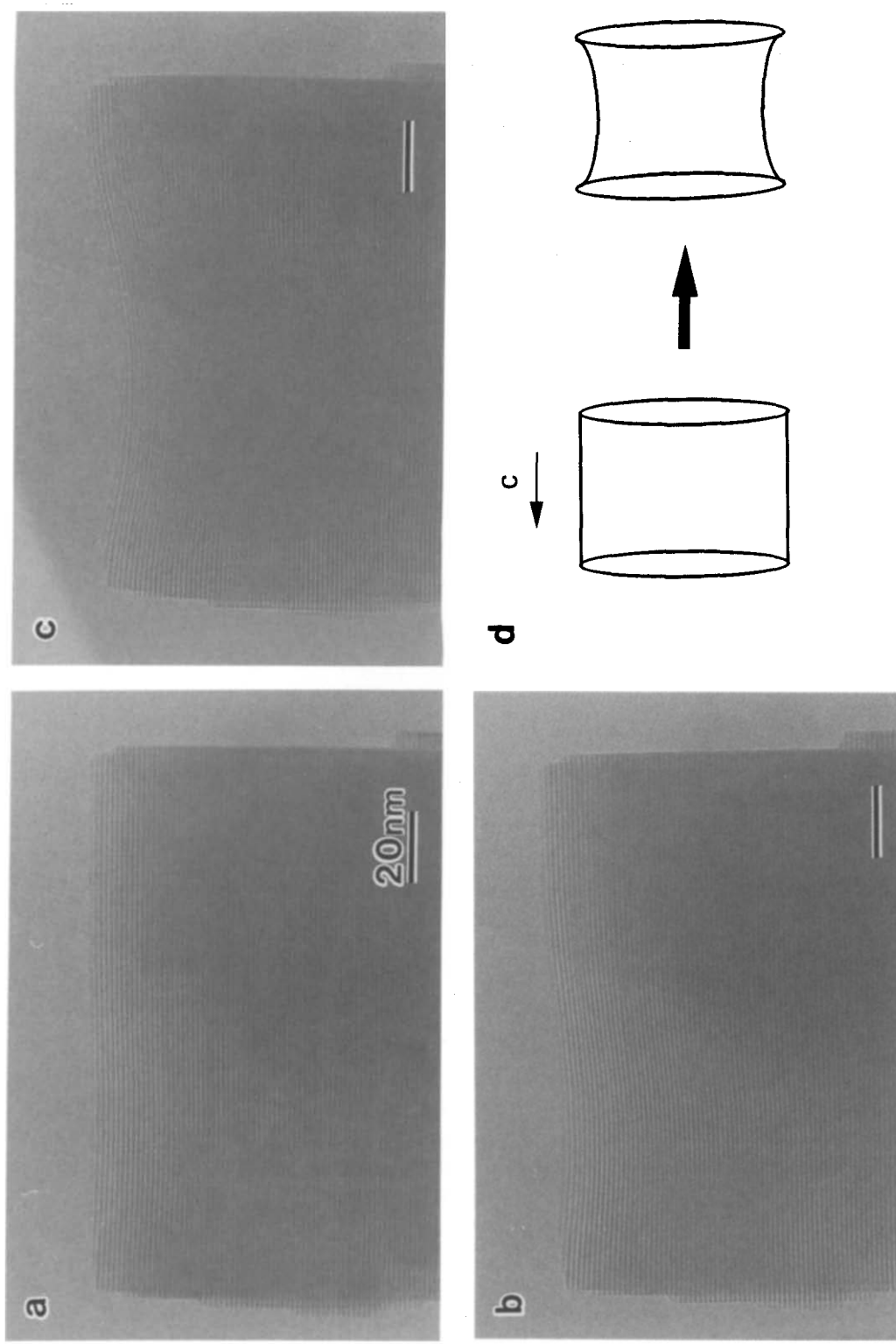

Fig. 4. A sequence of HRTEM images of LTL taken on 400 kV EM with [100] in order to show anisotropic damage under electron beam (a, b and c). Schematic drawing of c (d).

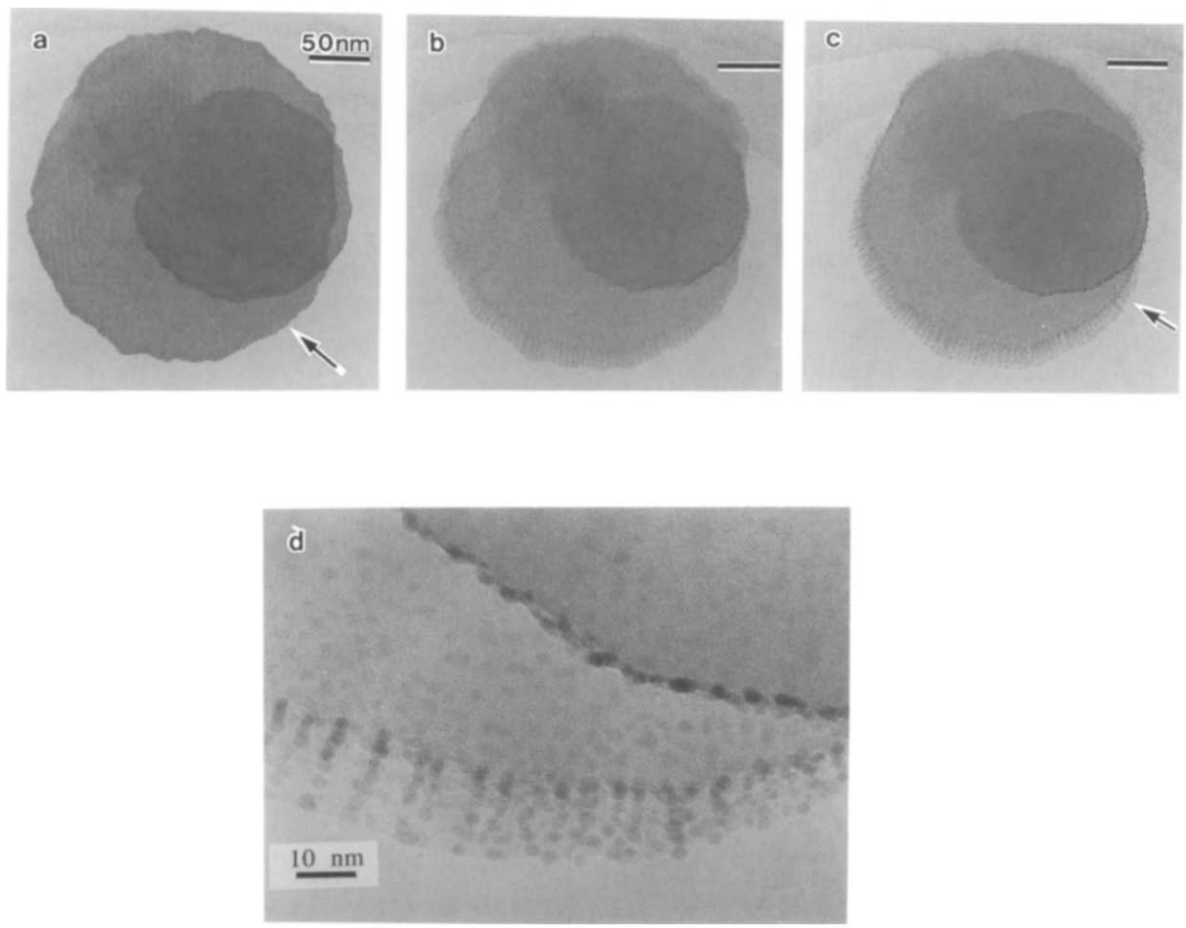

Fig. 5. A sequence of HRTEM images of Pt/LTL taken on 400 kV EM with [001] (a, b and c). (d) is an enlarged image of a part indicated by an arrow in (c).

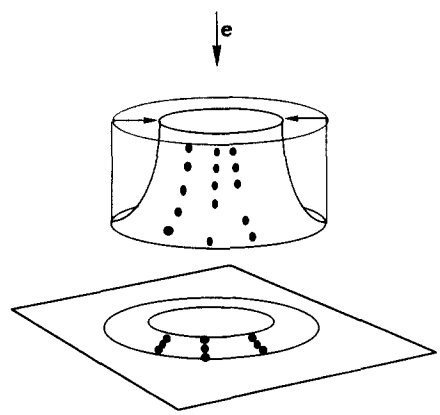

Fig. 6. A schematic drawing of the situation shown in Fig. 5. Diameter of the top shrinks due to the electron-irradiation effect.

by an electron beam is different from the previous type shown in Fig. 4. It is rather difficult to verify that the contrast observed for Pt/LTL in Fig. 5a is caused by the Pt particles on the (001), unless the framework is partly or completely destroyed by the beam as shown in Fig. 5b and c. However, Pt clusters, which are sticking to the side-wall of the crystals, i.e., {100}, show a clear contrast indicated by an arrow in Fig. 5a. Furthermore a strong tendency of aligning along the channels in the {100} surface is clearly traced through the morphology change of LTL under the beam by the series of images. An enlarged image of Fig. 5c is shown in Fig. 5d. This feature is schematically shown in Fig. 6.

Fig. 7a, b and c shows another set of sequential HRTEM images taken with the electron beam perpendicular to the channels. Pt particles are stationary on the surface during the electron beam irradiation and this is different from the previous observation of metallic particles [19]. The Pt particles, with a diameter of ca. 10–15 Å, are situated on the (001) surface. They can be seen situated above the row of channel openings at the surface in the projection shown in Fig. 7a. It is clear from all the observations that 10–15 Å Pt particles are easily detectable and that there is a spatial correlation between the channels and Pt particles (a few of them are shown by arrows in Fig. 7a). These Pt particles may be usable as electric lead (contact) for confined materials in the spaces. The shape and darkness of the contrast from the different rows of Pt particles indicates that the occupancy is not the same for each row, and a slight off-set can be seen in some cases. The degradation of the LTL framework, i.e. a serious damage by the electrons, is very clear from Fig. 7a–c. One can see the lattice fringes of Pt particles in both Fig. 7b and c, and it is quite obvious that the K-LTL crystal changes its morphology and the Pt particles migrate and change their sizes due to the influence of the beam. Therefore one must be careful to examine the particle size from the HRTEM image after the destruction of the framework, although it is easier to observe contrast from the particles.

3.2.2. *MFI system*

In this section, we want to stress the advantage of using high voltage EM for HRTEM image observation of the fine structures from thick specimens. The problem to be solved was to explain the discrepancies in the external surface area estimated by two different methods, the SEM image and the gas adsorption measurement. The crystals were too large to be imaged by 200 kV EM. HVHRTEM images of zeolites as-synthesized, a few microns in size, can provide information about the morphology and crystallographic orientational relationships of aggregates. The use of HVHRTEM will become more important especially in the observation of grain boundaries in membrane zeolites or in sintered zeolites without destruction. Fig. 8 shows HRTEM image of ZSM-5 (MFI type) with $SiO_2/Al_2O_3 = 70$, distributed by the Catalysis Society of Japan. The crystal consists of many crystallites, which stick together with the same orientation, and we can even observe very small differences in their orientation from the Moiré fringes, which are seen in some parts, due to the interference effect from two overlapping crystals [10].

3.2.3. *FAU system*

3.2.3.1. FAU as-synthesized. The structure of FAU consists of a three-dimensional cubic arrangement of large supercages (ca. 13 Å diameter) connected by 12-ring windows (ca. 7.2 Å diameter). The ideal framework structure of FAU has a space group $Fd\bar{3}m$ with lattice parameter $a = 24.7$ Å. It is constructed from sodalite cages which are linked via D6R to four other sodalite cages in such a way that all the sodalite cages are related by inversion at the centres of the D6Rs. The spatial arrangement of the sodalite cages is the same as the arrangement of carbon atoms in the diamond type and results in the large cages known as supercages with diameter ca. 13 Å. The relation of these supercages to one another has a diamond configuration with 12 T-atom rings connecting the cages. If we consider the pore system in the FAU structure to be that of channels rather than linked cages then these channels are of a zigzag nature with the smallest constriction ca. 6.9×7.4 Å. For the purposes of electron microscopic imaging these channels are observed along the $\langle 110 \rangle_c$ direction (subscript c and h refer to the cubic and hexagonal structure, respectively). The stacking of channels in the FAU structure is ABCABC (see the footnote of ref. [5] for a more precise description) along the $[111]_c$ direction.

We have looked at many zeolites including FAU and have found their lifetimes to be quite different depending on their sources, irrespective of the different Si/Al ratios of the framework. The presence of water in the crystal especially shortens

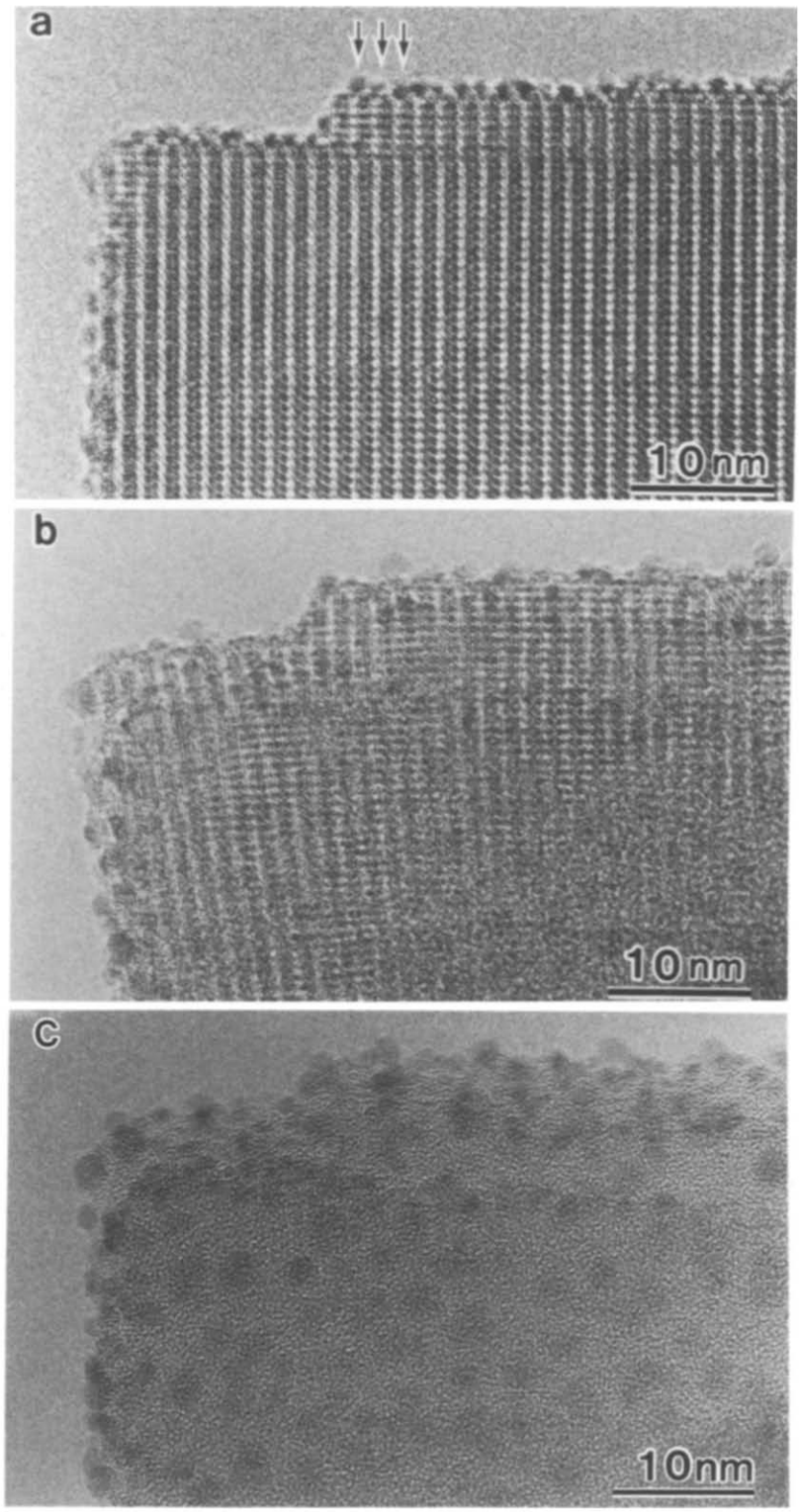

Fig. 7. A sequence of HRTEM images of Pt/LTL taken on 400 kV EM with [100].

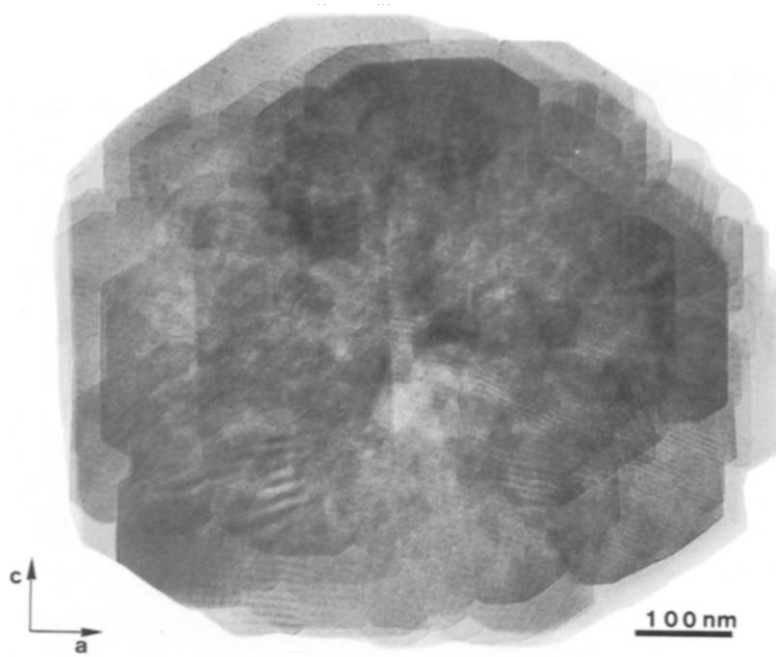

Fig. 8. An HRTEM image of Na-ZSM-5 taken on 1 MV EM. A whole crystal consists of many crystallites.

the lifetime of crystalline under the electron beam. Therefore for a long time we were very keen to remove water from the crystal before observation. We thought that this would surely improve the situation greatly, but now we realized that the most important factor for stability was the quality of their crystallinities. We can observe extremely beautiful HRTEM images even from fully hydrated ordinary Na-FAU (Si/Al=2.8) as shown in Fig. 9. The crystals as-synthesized are dispersed in water and dropped on a grid without any alteration prior to the observation. The dark contrast at the centres of the channels is due to an electron optical artifact which will be discussed in Section 3.2.5. The same crystals are used for surface structure observation (see Section 3.2.3.3). A crystal with good crystallinity shows mostly nice crystal morphology which is either in an equilibrium form or a growth form, even though the crystal size is small, for example ca. 1 μm. Zeolites are synthesized under supersaturation conditions, therefore we normally observe a growth form rather than an equilibrium form. The growth form is governed by the anisotropy of the growth rate which is sensitive to the growth conditions. By experience we believe that there is a strong correlation between thermal stability and the stability of the crystals under the electron beam. We therefore proposed a few years ago at the Annual Meeting of the Japanese Zeolite Association that the simplest way to find the crystal with a high thermal stability was to observe the beautiful morphology by SEM.

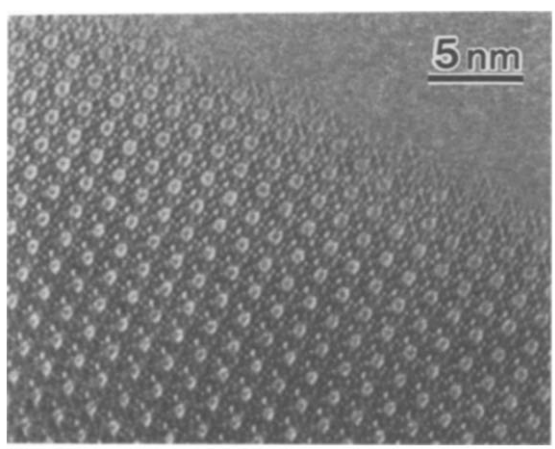

Fig. 9. An HRTEM image of a fully hydrated FAU taken on 400 kV EM with [110].

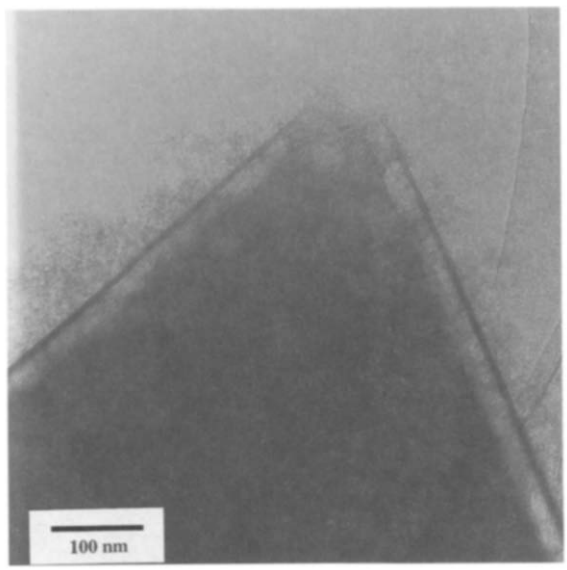

Fig. 10. An HRTEM image of dealuminated FAU by ammonium hexafluorosilicate taken on 400 kV EM with [110].

3.2.3.2. Dealumination of FAU Dealumination is a well-established technique for improving thermal stability and enhancing the acidity of zeolites. We were able to remove almost all the Si atoms from the framework by acid treatment followed by heat treatment, and were able to observe large mesopores and amorphous layers at the crystal surface, both of which were produced by the process [20]. Starting from the very regular octahedral shape of FAU, the crystals were mildly dealuminated by hexafluorosilicate in order to observe the process in an 'atomic' scale, and the observation of the initial stage of dealumination was possible only by observing the HRTEM image. The details of the specimen preparation and the experimental results will be published elsewhere [21]. An example of HRTEM images is shown in Fig. 10. The prominent features observed by HRTEM are summarized as follows: (i) amorphous layers are formed which follow the original crystal shape, (ii) many mesopores are formed between the amorphous layers and the crystals, (iii) mesopores are bounded on all sides by $\{111\}_c$ surfaces, and (iv) defects are preferentially attacked. Work is currently taking place to study whether the amorphous layers in Fig. 10 are Al-rich or Si-rich by using a modern EM with analytical equipment.

3.2.3.3. Surface structure and crystal growth units. In order to gain a better understanding of the chemical reaction occurring at the surface, the surface structure is the most important factor to be studied. Observation of the growth steps on an atomic scale will provide vital information about the crystal growth mechanism. Fig. 11a and b show HRTEM images to illustrate the growing steps at the surface, i.e. the surface structure of FAU taken with [110]. The height of these steps on the crystallite surface is basically equal to the spacing of $(111)_c$ FAU, i.e., one faujasite sheet. The image is so clear that it is possible to determine the nature of the terminating structures at the crystal faces by comparing them with simulated images. The following three different terminating surface models for FAU were simulated using the multi-slice method: (I) with an incomplete sodalite cage, (II) with a complete sodalite cage, and (III) with a complete D6R. These models are schematically shown in Fig. 12. At the top are the crystal surfaces. The simulated images of the type I surface fit very closely to the images of Fig. 11 and they are inserted in the figures. While another HRTEM image of FAU synthesized by a different method fits the simulated image of the type III surface. We have therefore observed two different types of surface, that is, structures (I) and (III)

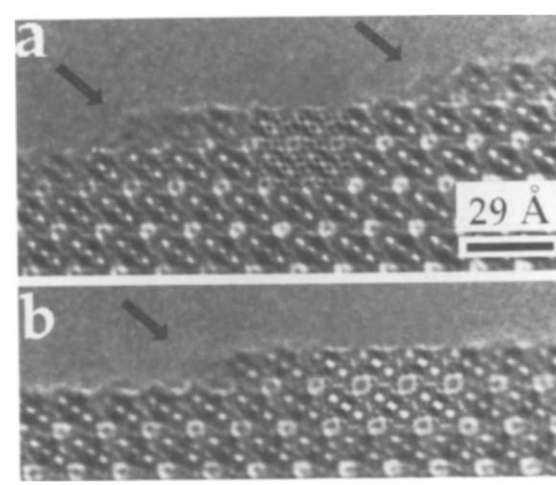

Fig. 11. HRTEM surface profile images of $\{111\}_c$ of FAU taken on 400 kV EM along $[110]_c$. Simulated images (specimen thickness of 50 Å) for the surface model I and focus of −900 Å (a) and −700 Å (b) are inserted.

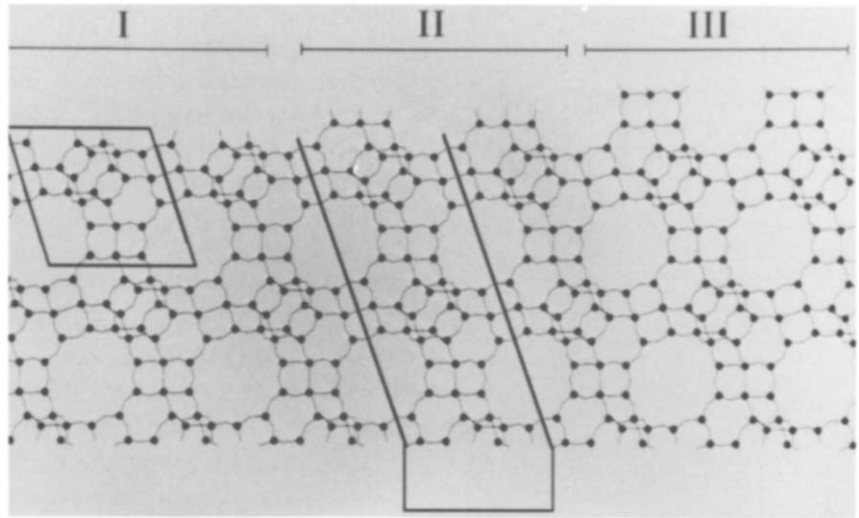

Fig. 12. Three different surface structure models for the $\{111\}_c$ surface of FAU viewing along $[110]_c$.

in FAU. Both have the common feature that they are incorporated with completed D6R. Structure (II), on the other hand, consists of a S6R at the surface. We propose therefore that the D6R is an important unit in the growth for FAU [22,23]. This does not necessarily mean that the crystal is formed by the unit of D6R from the gel. Different polymeric molecules may adsorb and desorb with their lifetimes. However once D6R is formed at the surface step, this is so stable that it will not desorb and the step advances to the next. D6R is the key unit for the crystal growth of FAU and Si/Al ordering of the framework.

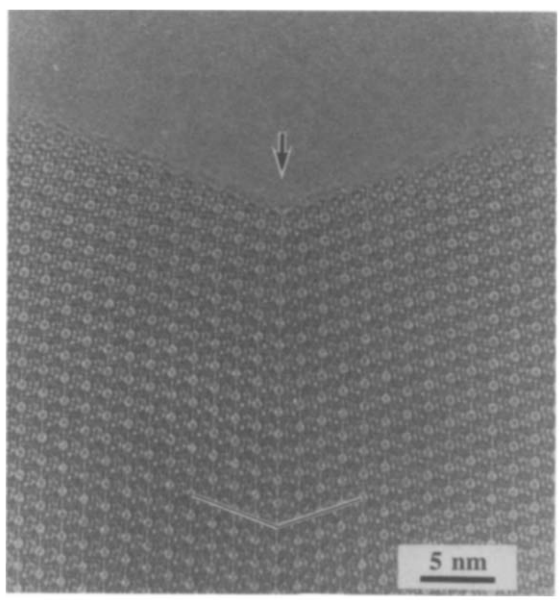

Fig. 13. An HRTEM image of a twin in FAU taken on 400 kV EM. Hexagonal arrangement is clearly visible at the twin boundary.

3.2.3.4. Oscillatory growth. The framework of EMT has hexagonal symmetry with lattice parameters $a = 17.4$ Å and $c = 28.4$ Å. This was first synthesized by Delprato et al. using the crown ether 18-crown-6 as a structure directing template [24]. Similar to the FAU framework, EMT is constructed from sodalite cages connected through D6Rs, however, one of the four connections, i.e. along the c-axis, is related by a mirror operation. Therefore, if there is a (111) twin plane in FAU through the centres of D6R then the structure changes to EMT locally. Twin is very common in FAU, and an HRTEM image of the twin in FAU is shown in Fig. 13, where the twin plane is indicated by an arrow and other two $\{111\}_c$ planes by lines. In FAU there are four independent $\langle 111\rangle_c$ directions along which EMT may intergrow, but one direction of four is chosen in the synthesis using the mixture of crown-ethers of 18-crown-6 and 15-crown-5 [5,23]. By viewing

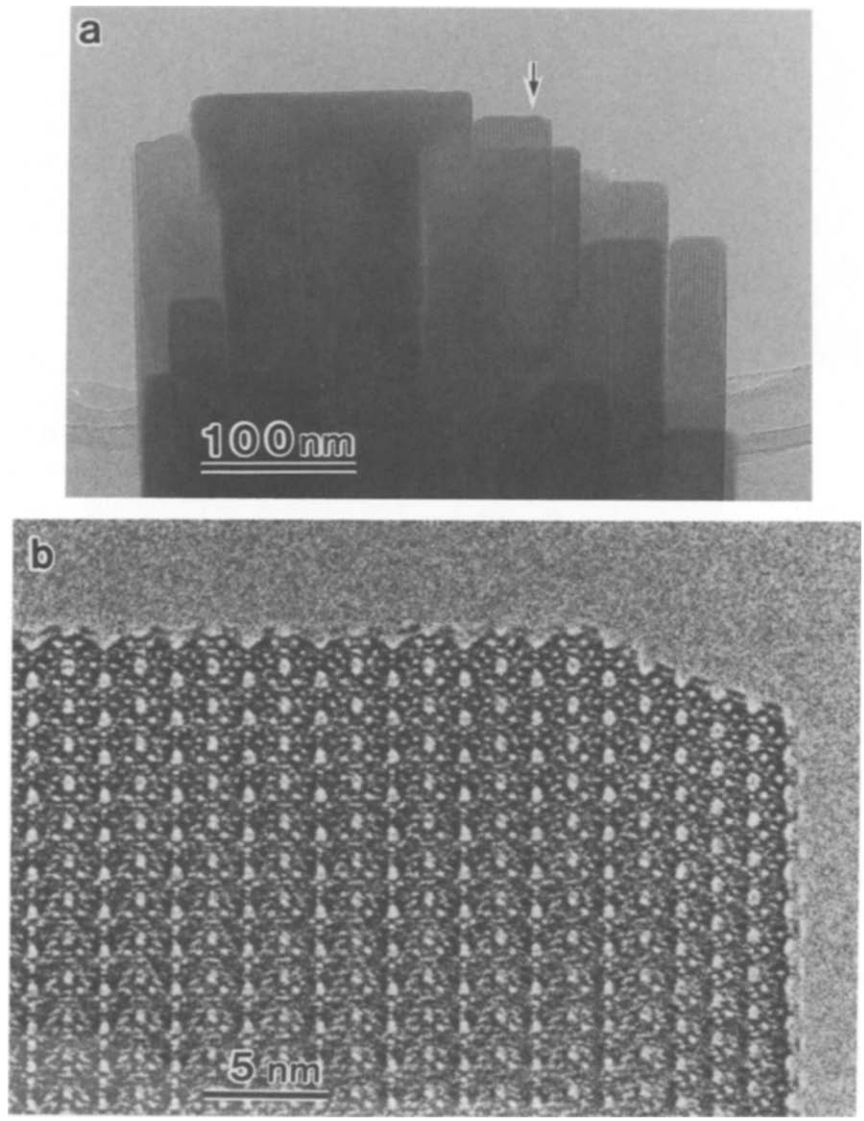

Fig. 14. An HRTEM image of EMT/FAU taken on 400 kV EM with $[110]_c$ or $[100]_h$. (b) is an enlarged image of a part of (a).

down $\langle 110 \rangle_c$ or $\langle 100 \rangle_h$ it is possible to distinguish between FAU and EMT. In intergrowth structures these two directions are coincident. In order not to describe the growth mechanism but these structures (D6R is the key unit for crystal growth, see the previous section), it is useful to construct the frameworks by stacking sheets so-called 'faujasite sheets'. If a pair of sheets are related by an inversion centre then the FAU framework is obtained. Conversely, if a pair of sheets are related by a mirror plane then the EMT framework is obtained.

During this study, we have observed oscillatory growth which may be related to the Liesegang ring of gel formation. Fig. 14a shows an example of oscillatory growth of the intergrowth in an extreme case. An enlarged image of a part of Fig. 14a (indicated by an arrow) is shown in Fig. 14b. There are many crystallites and all the EMT regions are sandwiched by FAU regions. Even though the specimen thickness is large, we can observe the fine details of the surface structure mentioned in the previous section.

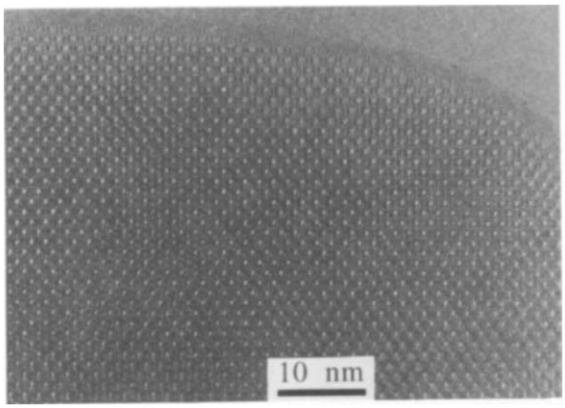

Fig. 15. An HRTEM image of Fe_2O_3/FAU taken on 400 kV EM with $[110]_c$.

3.2.3.5. Metal-oxides in the spaces, MoO_3 and Fe_2O_3 in FAU. There have been many trials aimed at incorporating metal or metallic compounds particles into the spaces. One method is to incorporate volatile compounds followed by a chemical reaction. Molybdenum oxide and iron oxide clusters were synthesized in the spaces of FAU by a few cycles of oxidation of adsorbed $Mo(CO)_6$ and $Fe_2(CO)_5$ in a closed circulation system at ca. 100°C or by UV light under oxygen pressure. Four MoO_3 and three (maximum may be five) Fe_2O_3 clusters per supercage were successfully fabricated in the spaces of FAU, respectively. This is a collaborative work with Dr. Y. Okamoto of Osaka University, Japan. The most important part of this study, from a structural point of view, is the confirmation that the framework structure is not destroyed by this treatment and that no surface precipitates are observed on the external surfaces. An HRTEM image of FeO_x/FAU (Fig. 15) clearly shows iron oxides, perhaps Fe_2O_3, clusters are incorporated into the spaces without any serious damage in the framework structure. This is direct evidence of the success of the incorporation by this method.

3.2.4. Si/Al concentration modulation in MOR

During the study of making an isolated Se chain into the one-dimensional channels of synthetic MOR, we observed an unusual black and white band contrast in the HRTEM image (Fig. 16). This peculiar contrast was determined as an amplitude contrast due to modulation of the Se content along b axis [25,26]. It has been shown from our recent optical absorption spectra of Se confined in the spaces that a finite number, 10–20, atoms of Se are physically adsorbed at each dipole induced by AlO_4^- and the cation [27]. Se atoms can be used as probes to detect the compositional variation of Al in the framework on the unit cell size by producing contrast in the HRTEM images [28]. The crystal MOR used has a plate-like character, wide along the b axis and thin along the c axis. This is quite different from natural MOR which is needle-shaped along the c axis. Compositional modulation may be responsible for this characteristic shape, through a dependence of the crystal growth rate (anisotropic) on the Si/Al ratio.

3.2.5. Artificial effects in imaging

To obtain the intuitive HRTEM images, in which the contrast is proportional to the projected potential for electrons, it might be necessary to

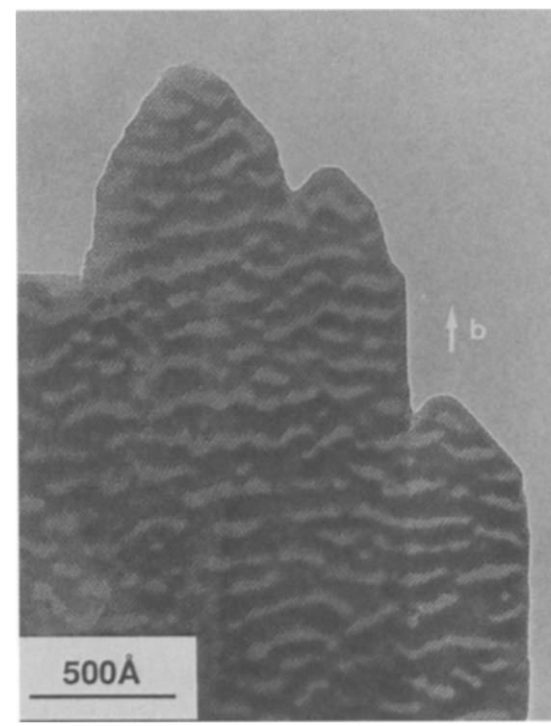

Fig. 16. An HRTEM image of Se-MOR taken on 200 kV EM with [001].

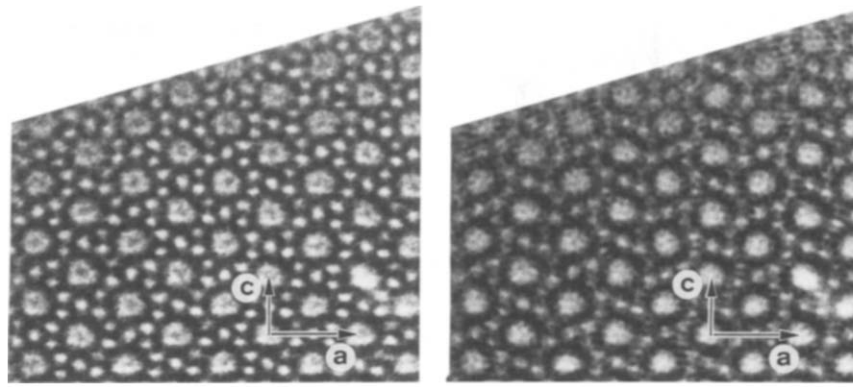

Fig. 17. An HRTEM image of silicalite taken along [010] on 400 kV EM using an objective aperture of 1.0 $Å^{-1}$ (left). The same image after image processing with the Wiener filter method (right).

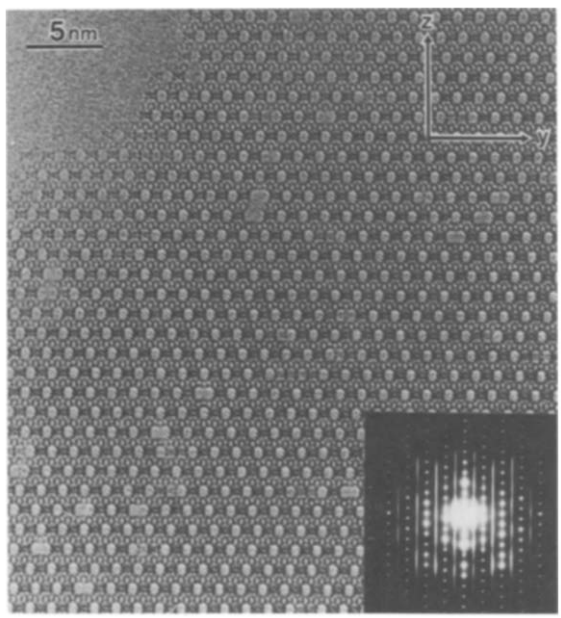

Fig. 18. An HRTEM image of ETS-10 along the x- (or y-axis) taken on 400 kV EM. The corresponding ED pattern is inserted at the bottom right of the figure.

have an EM with better resolution. The resolution of an electron microscope is essentially determined by the contrast transfer function which is a function of C_s, the spherical aberration coefficient of an objective lens, and λ the wave length of the incident electron. Information at small wave numbers, which is most important for image formation in zeolites with a large lattice constant, is inevitably less transferred as the resolution of EM becomes higher. This causes an artificial contrast at the centres of channels in the HRTEM images. It is therefore vitally important to distinguish this contrast from that of the materials confined in the spaces of the zeolites [10–12]. By knowing the origin of the artifacts we can remove artificial

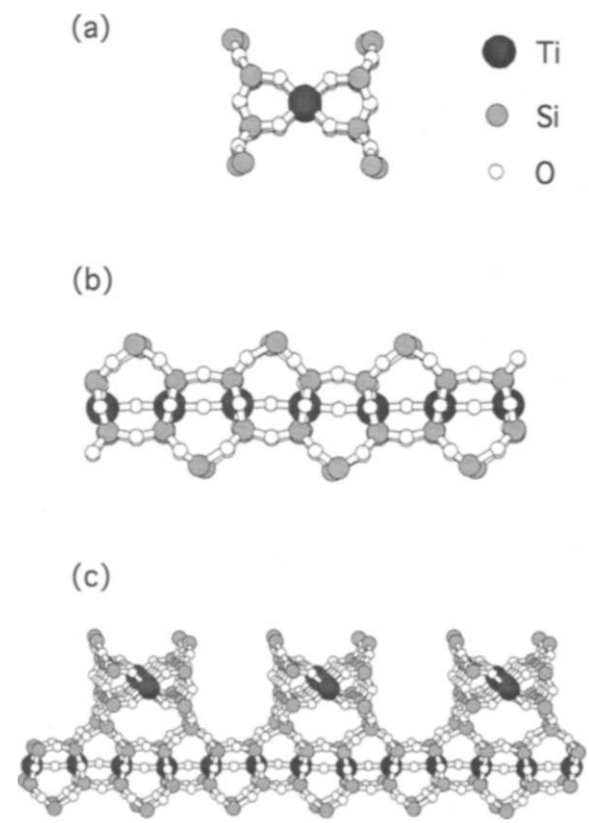

Fig. 19. Schematic diagrams of the rod structure. (a) Top view, (b) side view and (c) a manner of the connectivity.

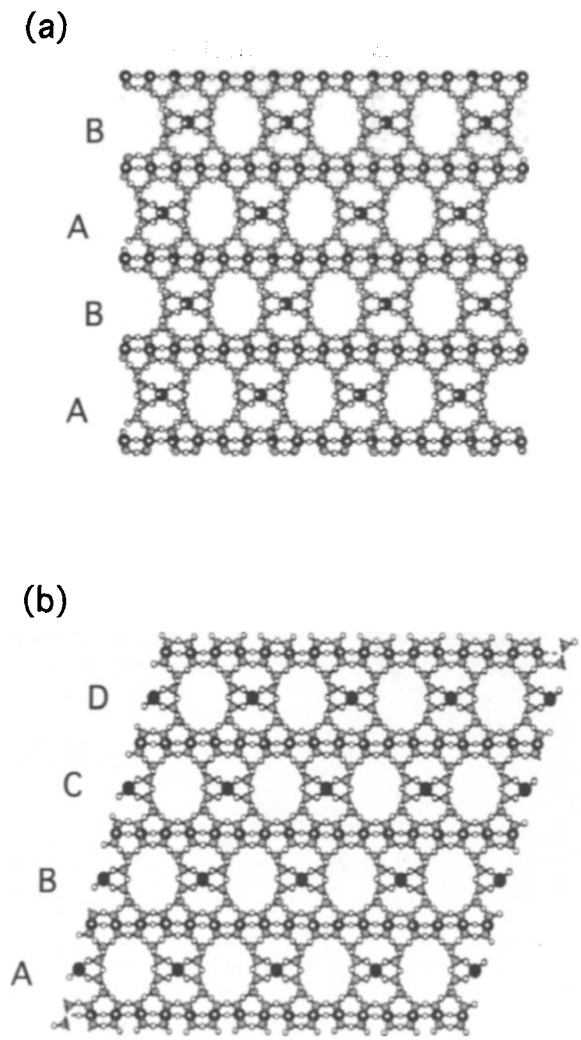

Fig. 20. Projected structure models for the structures of two end members, (a) polymorph A (ABAB stacking) and (b) polymorph B (ABCD stacking).

contrast with an image process. An example is shown for an HRTEM image of MFI type in Fig. 17a and b. The image was taken by 200 kV EM. Another method to remove this artifact is to take an HRTEM image at a much lower defocus than optimal focus conditions in order to enhance the transfer function at small wave numbers as discussed in a previous paper [12].

3.2.6. New titanosilicate, ETS-10

A new microporous titanosilicate ETS-10 was first synthesized in 1989. This material shows adsorption characteristics similar to zeolites and consequently offers potential as a shape-selective catalyst [29] as well as a container, but the structure remained unsolved until recently.

The crystal structure was solved mainly by HRTEM images and ED patterns. The crystal has a 4-fold axis in projection along the z axis. An HRTEM image and corresponding ED pattern taken with the axis perpendicular to z (assigned the x axis) are shown in Fig. 18. HRTEM images and ED patterns taken along another axis perpendicular to both x and z (assigned the y axis) are basically the same as those shown in Fig. 18, and this corresponds to 4-fold symmetry in projection along the z axis. We can observe a few different types of fault in the image and diffuse streaks in the ED pattern. The rod model is derived to explain a basic unit and basic structure of the layer. A proposed structure of the rod and the connectivity relation is shown in Fig. 19. The Si, O and Ti are distinguished by the different sized spheres in the figure. The rod consists of a one-dimensional titanium oxide chain $(–O–Ti–O–Ti–O–)_n$ and two 3-membered rings with Si on either side. Many polymorphs of ETS-10 are observed in the HRTEM images, Fig. 20a and b show two end members of polymorphs in projection. Fig. 20a corresponds to an ABAB... stacking, has unit cell parameters $a=b=14.85$ Å, $c=27.08$ Å, and fits the tetragonal space-group $P4_122$ or $P4_322$. *This is a chiral crystal system*, i.e., there is a spiral channel with a 12-membered ring aperture which spirals along the c axis in a clockwise or anticlockwise direction. Possibilities of lower symmetries, i.e. $P4_1$ and $P4_3$ must be carefully checked. Another ordered polymorph is shown in Fig. 20b and corresponds to an ABCD... stacking, has unit cell parameters $a=b=21.00$ Å, $c=14.51$ Å, $\beta=111.12°$, and fits the monoclinic space-group C2/c. In this polymorph a straight 12-membered ring channel runs parallel to the c axis [7,8,30,31]. A full paper concerning the EM study will be published separately [32].

Acknowledgements

The authors would like to extend their deep gratitude to D. Watanabe, S. Andersson, J.M. Tho-

mas, the late J.V. Sanders, J.-O. Bovin, V. Alfredsson, M.W. Anderson and Y. Nozue for their continuous support, collaboration and encouragement. Thanks are also due to Dr. Y. Okamoto for supplying metal oxide/FAU specimens and to Y. Nakaizumi (Hitachi, japan) for giving us the opportunity to use the most advamced SEM. OT thanks Grant in Aid from a new program of the Ministry of Education, Science and Culture, Japan, and the British Council for support. Sumitomo Chemical Co. and Nippon Sheet Glass Foundation for Material Science are also acknowledged for partial support.

References

[1] D.W. Breck, Zeolite Molecular Sieves, Wiley, New York, 1974.

[2] G.R. Millward, S. Ramdas and J.M. Thomas, On the direct imaging of offretite, cancrinite, chabazite and other related ABC-6 zeolites and their intergrowths, Proc. Roy. Soc., A399 (1985) 57–71.

[3] G.R. Millward, J.M. Thomas, O. Terasaki and D. Watanabe, Direct imaging and characterization of intergrowth-defects in erionite, Zeolites 6 (1986) 91–95.

[4] M.W. Anderson, K.S. Pachis, F. Prebin, S.W. Carr, O. Terasaki, T. Ohsuna and V. Alfredsson, Intergrowths of cubic and hexagonal polytypes of faujasitic zeolites, J. Chem. Soc., Chem. Commun., (1991) 1660–1664.

[5] O. Terasaki, T. Ohsuna, V. Alfredsson, J.-O. Bovin, D. Watanabe, S.W. Carr and M.W. Anderson, Observation of spatially correlated intergrowths of faujasitic polytypes and the pure end members by high-resolution electron microscopy. Chem. Mater., 5 (1993) 452–458.

[6] J.M. Newsam, M.M.J. Treacy, W.T. Koetsier and C.B. Gruyter, Structural characterization of zeolite beta, Proc. Roy. Soc. (London), A420 (1988) 375–405.

[7] M.W. Anderson, O. Terasaki, T. Ohsuna, A. Philippou, S.P. MacKay, A. Ferreira, J. Rocha and S. Lidin, Structure of the microporous titanosilicate ETS-10, Nature, 367 (1994) 347–351.

[8] M.W. Anderson, O. Terasaki, T. Ohsuna, A. Philippou, S.P. MacKay, A. Ferreira, J. Rocha and S. Lidin, Microporous titanosilicate ETS-10: A structural survey, Phil. Mag., (1995).

[9] L.A. Bursill, E.A. Lodge and J.M. Thomas, Zeolitic structures as revealed by high-resolution electron microscopy, Nature, 286 (1980) 111–113.

[10] O. Terasaki, T. Ohsuna, V. Alfredsson, J.-O. Bovin, D. Watanabe and K. Tsuno, The study of zeolites by HVHREM, Ultramicroscopy, 39 (1991) 238–246.

[11] V. Alfredsson, O. Terasaki and J.-O. Bovin, On crystal structure imaging of silicalite by HREM, J. Solid State Chem., 84 (1990) 171–177.

[12] V. Alfredsson, O. Terasaki and J.-O. Bovin, The conditions for detecting confined material in the channels/cavities of zeolites by using HREM, J. Solid State Chem., 105 (1993) 223–233.

[13] O. Terasaki, J.M. Thomas and G.R. Millward, Imaging the structures of zeolite L and synthetic mazzite, Proc. Roy. Soc. (London), A395 (1984) 153–164.

[14] O. Terasaki, HREM study of the fine structures of zeolites and materials confined in their spaces: Are zeolites good enough as containers for confined materials? J. Solid State Chem., 106 (1993) 190–200.

[15] M.M.J. Treacy and J.M. Newsam, Electron beam sensitivity of zeolite L, Ultramicroscopy, 23 (1994) 411–420.

[16] V. Alfredsson, O. Terasaki, Z. Blum, J.-O. Bovin and G. Karlsson, The platinum agglomeration in the {111}-twin planes of zeolite FAU, Zeolites (1995).

[17] M.M.J. Treacy, A. Howie and C.J. Wilson, Z contrast of platunum and palladium catalysis, Phil. Mag., A38 (1978) 569–585.

[18] S.B. Roce, J.Y. Koo, M.M. Disco and M.M.J. Treacy, On the imaging of Pt atoms in zeolite frameworks, Ultramicroscopy, 34 (1990) 108–118.

[19] R. Wallenberg, J.-O. Bovin and D.J. Smith, Atom hopping on small gold particles imaged by high-resolution electron microscopy, Naturwiss. S., 72 (1985) 539–541.

[20] H. Horikoshi, S. Kasahara, T. Fukushima, K. Itabashi, T. Okada, O. Terasaki and D. Watanabe, Study of mesopores induced by dealumination in zeolite Y, J. Chem. Soc., Jpn. Chem. Ind. Chem., (1989) 398–404.

[21] T. Ohsuna, O. Terasaki, D. Watanabe, M.W. Anderson and S.W. Carr, Hexagonal (EMT)/cubic (FAU) zeolite intergrowth materials: A SEM and HRTEM study, Chem. Mater., 6 (1994) 2201–2204.

[22] V. Alfredsson, T. Ohsuna, O. Terasaki and J.-O. Bovin, Investigation of the surface structure of the zeolite FAU and EMT by high-resolution transmission electron microscopy, Angew. Chem. Int. Ed. Engl., 32 (1993) 1210–1213.

[23] T. Ohsuna, O. Terasaki, V. Alfredsson, J.-O. Bovin, D. Watanabe, S.W Carr and M.W. Anderson, Observation of fine structure in FAU, EMT and intergrowth crystals by high-resolution electron microscopy, submitted for publication.

[24] E. Delprato, L. Delmotte, J.L. Guth and L. Huve, Synthesis of new silica-rich cubic and hexagonal faujasite using crown-ether-based supramolecules as templates, Zeolites, 10 (1990) 546–552.

[25] O. Terasaki, K. Yamazaki, J.M. Thomas, T. Ohsuna, D. Watanabe, J.V. Sanders and J.C. Bary, Isolating individual chains of selenium by incorporation into the channels of a zeolite, Nature, 330 (1987) 58–60.

[26] O. Terasaki, K. Yamazaki, J.M. Thomas, T. Ohsuna, D. Watanabe, J.V. Sanders and J.C. Bary, The incorporation of selenium into the channels of mordenite: An electron microscopic study, J. Solid State Chem., 77 (1988) 72–83.

[27] Y. Nozue, T. Kodaira, O. Terasaki, K. Yamazaki, T. Goto, D. Watanabe and J.M. Thomas, Absorption spectra of selenium clusters and chains incorporated into zeolites, J. Phys. Condens. Matter, 2 (1990) 5209–5217.

[28] O. Terasaki, Study of the fine structure of zeolites and materials confined in zeolites, Acta Chem. Scand., 45 (1991) 785–790.

[29] S.M. Kuznicki, K.A. Thrush, F.M. Allen, S.M. Levine, M.M. Hamil, D.T. Hayhurst and M. Mansour, in M.L Occelli and H. Robson (Editors), Molecular Sieves, Van Nostrand–Reinhold, New York, 1992, pp. 437–453.

[30] O. Terasaki, T. Ohsuna, V. Alfredsson, J.-O. Bovin, S.W. Carr, M.W. Anderson and D. Watanabe, Fine structures of zeolites: Defects, interfaces and surface structures. An HREM study, in Zeolites and Microporous Crystals, Kodansha, Tokyo, 1994, pp. 77–84.

[31] T. Ohsuna, O. Terasaki, D. Watanabe, M.W. Anderson and S. Lidin, Microporous titanosilicate ETS-10: Electron microscopy study, in J. Weitkamp, H.G. Karge, H. Pfeifer and W. Hölderich (Editors), Zeolites and Related Microporous Materials: State of the Art 1994, Elsevier, Amsterdam, 1994, pp. 413–420.

[32] O. Terasaki, T. Ohsuna, M.W. Anderson, A. Ferreira, J. Rocha, S. Lidin and D. Watanabe, to be submitted.